The Astrophysical Journal, 700:1391–1403, 2009 August 1 doi:10.1088/0004-637X/700/2/1391

EMERGENCE OF SMALL-SCALE MAGNETIC LOOPS THROUGH THE QUIET SOLAR ATMOSPHERE

M. J. Martínez González[1,3] and L. R. Bellot Rubio[2]
[1] Instituto de Astrofísica de Canarias, C/Vía Láctea s/n, 38200 La Laguna, Tenerife, Spain; marian@iac.es
[2] Instituto de Astrofísica de Andalucía (CSIC), Apdo. 3004, 18080, Granada, Spain
Received 2009 February 6; accepted 2009 May 19; published 2009 July 14

ABSTRACT

We investigate the emergence of magnetic flux in the quiet Sun at very small spatial scales, focusing on the magnetic connection between the photosphere and chromosphere. The observational data consist of spectropolarimetric measurements and filtergrams taken with the *Hinode* satellite and the Dutch Open Telescope. We find that a significant fraction of the magnetic flux present in internetwork regions appears in the form of Ω-shaped loops. The emergence rate is 0.02 loops per hour and arcsec^{-2}, which brings 1.1×10^{12} Mx s^{-1} arcsec^{-2} of new flux to the solar surface. Initially, the loops are observed as small patches of linear polarization above a granular cell. Shortly afterward, two footpoints of opposite polarity become visible in circular polarization within or at the edges of the granule and start moving toward the adjacent intergranular space. The orientation of the footpoints does not seem to obey Hale's polarity rules. The loops are continuously buffeted by convective motions, but they always retain a high degree of coherence. Interestingly, 23% of the loops that emerge in the photosphere reach the chromosphere (16 cases out of 69). They are first detected in Fe I 630 nm magnetograms and 5 minutes later in Mg I b 517.3 nm magnetograms. After about 8 minutes, some of them are also observed in Ca II H line-core images, where the footpoints produce small brightness enhancements.

Key words: polarization – Sun: atmosphere – Sun: magnetic fields

Online-only material: mpeg animation

1. INTRODUCTION

It is believed that solar magnetic fields are created in the tachocline, the interface between the convection zone and the radiative interior. Due to buoyancy instabilities, they move upward and emerge into the solar atmosphere in the form of Ω-shaped flux tubes (Zwaan 1985). The largest emerging active regions produce sunspots with magnetic fluxes in excess of 10^{21} Mx and lifetimes of several weeks to months. Smaller active regions consist of pores and contain an order of magnitude less flux, persisting over days to weeks. The smallest emerging regions detected to date are the so-called ephemeral regions. They have fluxes between 10^{18} and 10^{20} Mx and lifetimes in the range from hours to days (e.g., Martin 1988; Martin & Harvey 1979; Hagenaar et al. 2003).

Outside of active regions, the quiet Sun has proved to be full of magnetic fields with strengths roughly in equipartition with the photospheric convective flows (Lites 2002; Khomenko et al. 2003; Domínguez Cerdeña et al. 2006; Orozco Suárez et al. 2007; Martínez González et al. 2008b). An important question is the origin of these fields. Lites et al. (1996) suggested that horizontal internetwork fields represent concentrated loops of flux carried to the surface by the upflows of granular convection or by magnetic buoyancy. In a recent paper, Martínez González et al. (2007) indirectly traced the emergence of magnetic flux and reconstructed, for the first time, the three-dimensional topology of the magnetic field vector in quiet regions of the solar photosphere. It was found that at least 20% of the magnetic flux in the quiet Sun is connected by low-lying magnetic loops. Later, Centeno et al. (2007) studied time series of spectropolarimetric observations taken with the Solar Optical Telescope aboard *Hinode*. These authors followed the time evolution of one magnetic loop in the internetwork, showing that they appear on spatial scales smaller than 2″. Ishikawa et al. (2007) and Ishikawa & Tsuneta (2009) demonstrated that the emergence of magnetic flux on granular scales brings large amounts of horizontal fields to the photosphere both in plage regions and in the quiet Sun. Another form of flux emergence has been reported by Orozco Suárez et al. (2008). It involves the appearance and subsequent disappearance of what seem to be vertical fields at the center of granular cells.

The observations strongly suggest that a significant fraction of the magnetic flux in the quiet Sun might be the result of the emergence of small-scale magnetic loops. But, where do the loops come from? Are they created by the global solar dynamo, by a local dynamo, or by recycling of the flux from decaying active regions? Is the emergence process a local phenomenon confined to the photosphere or does the magnetic flux reach higher atmospheric layers?

The answers to these questions bear important consequences for our understanding of the magnetic and thermal structure of the solar atmosphere. For example, Trujillo Bueno et al. (2004) claim that the magnetic energy stored in the quiet photosphere is sufficient to balance the radiative losses of the chromosphere. Quiet Sun magnetic fields are excellent candidates to solve the chromospheric and coronal heating problem, but a mechanism capable of transferring their energy to the upper layers has not been identified yet. From a theoretical point of view, it is not clear whether the fields of the quiet solar photosphere can rise to the chromosphere. Isobe et al. (2008) have presented MHD simulations in which the magnetic field emerges into the photosphere in the form of small-scale Ω-loops. They reach the chromosphere and get reconnected with the local expanding vertical magnetic fields, heating the plasma and generating high-frequency MHD waves that propagate into the corona. However, the magnetoconvection simulations of Stein & Nordlund (2006) show Ω-loops that disintegrate as they rise through the solar atmosphere.

[3] Formerly at Observatoire de Paris.

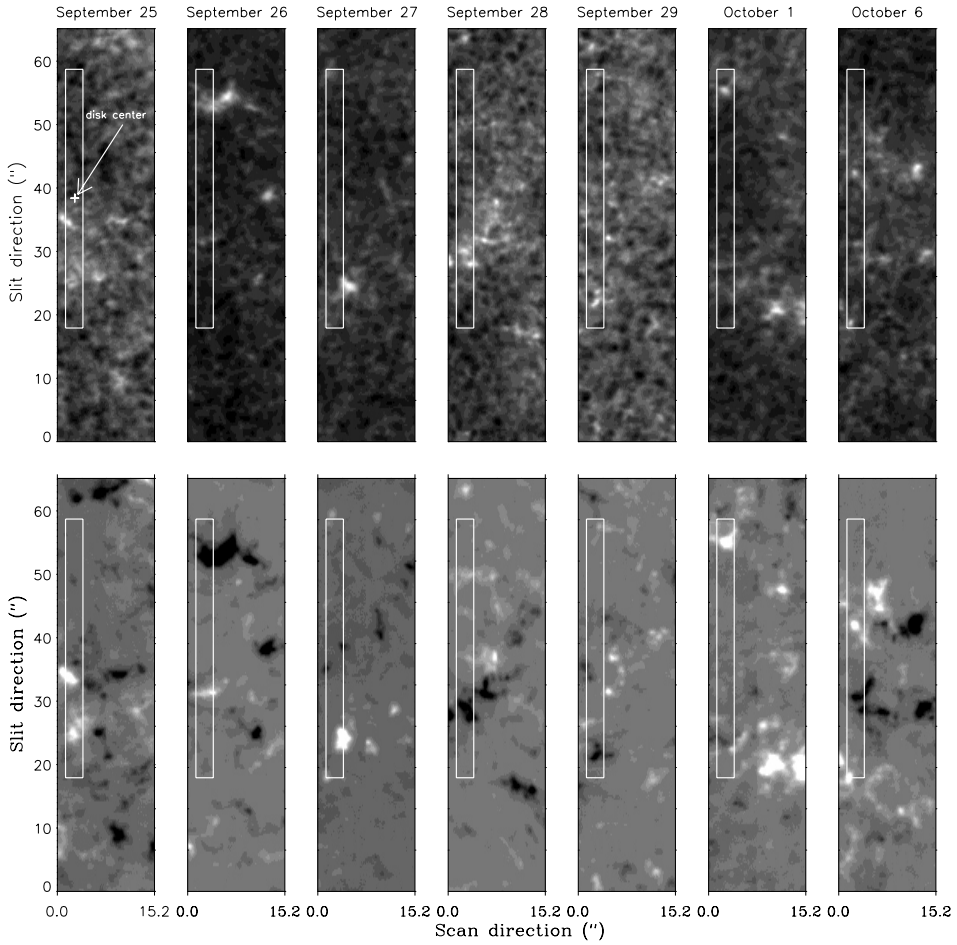

Figure 1. Quiet Sun regions observed during HOP 14. Top: Ca II H line-core maps averaged over each day. Bottom: same, for the Mg I b magnetograms. White and black represent positive and negative polarity magnetic fields, respectively. The white rectangles indicate the areas scanned with the SP. North is up and west to the right.

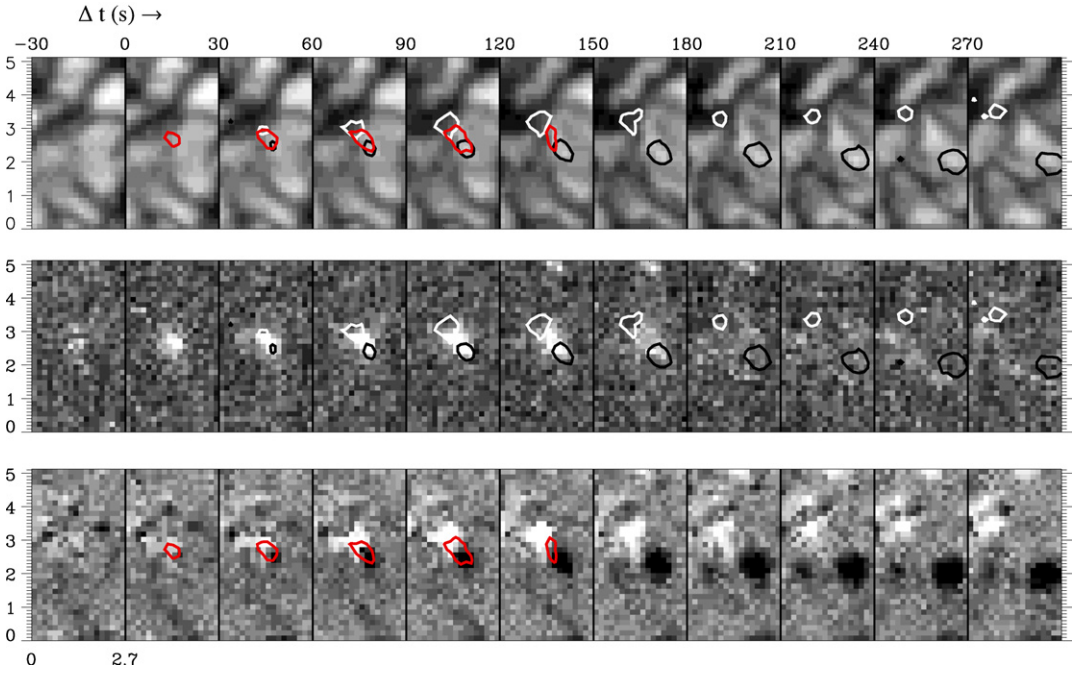

Figure 2. Emergence of a small-scale magnetic loop in the quiet solar photosphere. Time runs from left to right. Top: maps of continuum intensity at 630 nm. Middle: total linear polarization in the 630.25 nm line, saturated at 0.3 pm. Bottom: total circular polarization in the 630.25 nm line. The signals are clipped at ±0.1 pm. Red contours represent linear polarization larger than 0.22 pm. Black and white contours indicate circular polarization signals stronger than ±0.1 pm. Both *x*- and *y*-axis are in arcsec.

Table 1
Log of the Observations

Date	1st Period (UT)	2nd Period (UT)	Observed Time (hr)	Detected Loops
Sep 25	13:00–15:59		3.0	18
Sep 26	08:15–14:14		6.0	16
Sep 27	06:16–09:59	11:25–13:59	6.3	7
Sep 28	07:00–09:59	11:20–13:59	5.7	11
Sep 29	06:51–09:44		2.9	5
Oct 1	08:21–10:09		1.8	3
Oct 6	08:01–10:18		2.3	9

These discrepancies emphasize the need for observational studies aimed at determining whether magnetic fields emerging into the quiet photosphere are able to reach higher atmospheric layers. Here we use multi-wavelength observations taken by *Hinode* and the Dutch Open Telescope to address this question. We also characterize the physical properties of small-scale magnetic loops in the quiet Sun, providing estimates of their magnetic fluxes, emergence rates, lifetimes, sizes, and velocities.

2. OBSERVATIONS AND DATA REDUCTION

The data analyzed in this paper consist of time series of polarimetric and imaging observations of quiet Sun regions at the disk center. They were acquired in seven different days (September 25–29, 2007 October 1 and 6) using the instruments of the Solar Optical Telescope aboard *Hinode* (Kosugi et al. 2007) and the Dutch Open Telescope (DOT; Rutten et al. 2004) at Observatorio de El Roque de Los Muchachos (La Palma, Spain). The observations belong to the *Hinode* Operation Plan 14, entitled "*Hinode*/Canary Islands campaign."

The *Hinode* spectro-polarimeter (SP; Lites et al. 2001) recorded the full Stokes vector of the pair of Fe I lines at 630 nm in a narrow field of view (FOV) of $2\farcs7 \times 40\farcs6$. This region was scanned with a cadence of 28 s during 2–6 hr per day (Table 1). The exposure time per slit position was set to 1.6 s to track very rapid events. However, this mode of operation also led to a noise level of 1.7×10^{-3} in units of the continuum intensity I_c. With a pixel size of $0\farcs16$ along the slit and $0\farcs15$ perpendicular to it, the SP measurements have a spatial resolution of about $0\farcs32$.

The *Hinode* Narrowband Filter Imager (NFI; Tsuneta et al. 2008) acquired Stokes I and V filtergrams in the wings of the upper photosphere/transition region Mg I b 517.3 nm line, ± 11.5 pm away from its center. The NFI was operated in shutterless mode to reach an effective exposure time of 9.6 s per wavelength and polarization state, covering an FOV of $15\farcs4 \times 65\farcs3$. The original filtergrams had a pixel size of $0\farcs08$, but we rebined them to the SP pixel size in order to further reduce the noise. The *Hinode* Broadband Filter Imager (BFI; Tsuneta et al. 2008) acquired simultaneous images of the photosphere in the CN band head at 388.3 nm (filter width of 0.52 nm) and the chromosphere in the Ca II H line at 396.85 nm (a filter width of 0.22 nm). The exposure times were 0.1 s and 0.3 s, respectively. The BFI covered a region of $19\farcs2 \times 74\farcs1$ with a pixel size of $0\farcs055$. Both the NFI and the BFI took images with a cadence of 30 s.

The area scanned by the SP represents a small part of the total FOV of the NFI and the BFI. Therefore, we have co-spatial and co-temporal observations of the quiet Sun tracing different heights in the atmosphere.

The DOT observed photospheric and chromospheric layers by means of a tunable Lyot filter that scanned the intensity profile of the Hα line at five wavelength positions (± 0.7, ± 0.35, and 0 Å). The passband of the filter was 0.25 Å. Speckle bursts of 100 frames were taken at each wavelength position every 30 s. Following the standard reduction procedure at the DOT, the individual filtergrams were reconstructed using a speckle masking technique (see, Rutten et al. 2004 for details). The reconstructed images cover an FOV of $91\farcs2 \times 89''$ and have a spatial resolution of about $0\farcs2$. The DOT and *Hinode* carried out simultaneous observations, but there is little overlap between them because of bad weather conditions.

The SP data have been corrected for dark current, flat-field, and instrumental cross-talk using the sp_prep.pro routine included in the SolarSoft package. The algorithm applied to the *Hinode* filtergrams (fg_prep.pro) removed dark current, hot pixels, and cosmic rays. The spectropolarimetric maps and the various filtergrams have been aligned with pixel accuracy using the granulation, G-band bright points, and network elements as a reference.

In Figure 1, we show time-averaged Ca II H filtergrams and Mg I b magnetograms for the 7 days of observation. The Ca II H images have been trimmed to the size of the Mg I b FOV. The rectangles represent the areas scanned by the SP. Note the absence of strong brightenings in the Ca II H maps, as expected for very quiet regions largely devoid of network elements.

3. DATA ANALYSIS

3.1. Detection of Magnetic Loops in Different Layers

Loop-like magnetic structures leave clear signatures in spectropolarimetric maps: linear polarization flanked by two circular polarization signals of opposite polarity. One of the main goals of this paper is to trace the possible ascent of small-scale magnetic loops through the solar atmosphere. To this end, we use photospheric and chromospheric observables.

The SP data make it possible to investigate the topology of the field in the photosphere. The information is complemented by the CN filtergrams, where bright points associated with magnetic fields are easily visible. We define the total circular polarization as the integral of the unsigned 630.25 nm Stokes V spectrum. The integration is carried out in the wavelength range from -17.25 pm to +30.31 pm. The total linear polarization is computed as the integral of the Stokes $L = \sqrt{Q^2 + U^2}$ profile of Fe I 603.25 nm, using the same initial and final wavelengths.

We visually inspect the polarization maps to search for weak linear signals between two patches of circular polarization with opposite polarity. Since in general the linear polarization signals are very small in the quiet Sun, we ascribe those cases to loop-like structures only after corroborating that the linear polarization is produced by symmetric Stokes Q and U profiles.

Figure 2 shows the first stages of the emergence of a small-scale magnetic loop as seen in the Fe I 630.25 nm line. The different panels represent continuum intensity (top), total linear polarization (middle), and total circular polarization (bottom). Red contours indicate enhanced linear polarization. Black and white contours mark the location of strong negative and positive circular signals, respectively. At $\Delta t = 0$ s, a patch of linear polarization shows up at the center of the image. It corresponds to the horizontal part of a magnetic structure emerging into the photosphere. Between $\Delta t = 30$ and 60 s, two circular polarization patches of opposite polarity appear next to it, at the edge of a granular cell. The fact that the linear signal is detected earlier than the circular polarization indicates that the magnetic structure has the shape of an Ω-loop: the apex creates linear polarization and the vertical fields of the footpoints

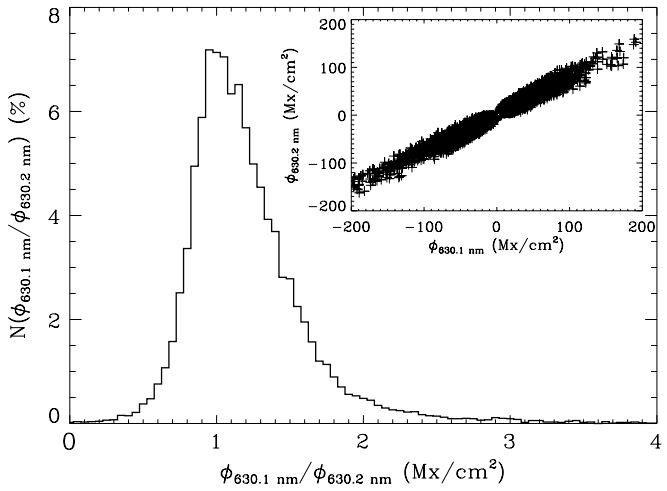

Figure 3. Histogram of the ratio between the magnetic flux density inferred from Fe I 630.15 nm and 630.25 nm. The inset shows a scatter plot of the values derived from the two spectral lines.

give rise to circular polarization (Centeno et al. 2007). The linear polarization disappears below the noise at $\Delta t \sim 150$ s while the footpoints separate with time. This sequence of events is consistent with a loop that emerges and travels up in the atmosphere. The distance between the footpoints keeps increasing until they reach the edges of the area scanned by the SP. The subsequent evolution of this loop will be studied in Section 4.1.

The Stokes I and V filtergrams acquired in the red and blue wings of the Mg I b line give information about the upper photosphere/temperature minimum region (Lites et al. 1988). We have used them to construct longitudinal magnetograms (M) and Dopplergrams (D) as

$$M = \frac{1}{2}\left(\frac{V_b}{I_b} - \frac{V_r}{I_r}\right) \quad (1)$$

$$D = \frac{I_r - I_b}{I_r + I_b}, \quad (2)$$

where the subscripts r and b represent the measurements at +11.5 and −11.5 pm from line center, respectively. To first order, the magnetograms computed in this way are not affected by mass motions. The quantities M and D have been transformed into magnetic flux densities and line-of-sight (LOS) velocities according to

$$\phi \approx 9063\, M, \quad (3)$$

$$v_{\rm LOS} \approx 10.48\, D - 0.28, \quad (4)$$

with ϕ in Mx cm^{-2} and $v_{\rm LOS}$ in km s^{-1}. Equation (4) is valid in the range $-2 < v_{\rm LOS} < 2$ km s^{-1}. These expressions have been obtained through the calibration of the Mg I b line shape in the Fourier Transform Spectrometer atlas of the quiet Sun (Brault & Neckel 1987) and give only rough estimates of the magnetic flux density and velocity at the height of formation of the Mg I b measurements. Since Stokes Q and U were not recorded, the Mg I magnetograms can only be used to detect relatively vertical fields such as those expected at/in the footpoints of magnetic loops. By definition, fields pointing toward the observer and upflows will both be positive. Note that our sign convention for the velocity differs from that commonly used in astrophysics.

In the chromosphere we do not have polarimetric information. However, magnetic fields can be detected through brightness enhancements in the Ca II H filtergrams. The passband of the *Hinode* Ca II H filter includes a significant photospheric contribution, but it has a long tail that extends well into the chromosphere (Carlsson et al. 2007). Finally, information on the upper chromosphere is provided by the Hα measurements taken at the DOT. We have used them to construct Dopplergrams at different heights in the chromosphere.

3.2. Photospheric Magnetic Flux

We determine the magnetic flux density from the Stokes V profiles of the Fe I 630 nm lines using the weak field approximation (e.g., Landi degl'Innocenti 1992)

$$V(\lambda) = -\phi\, C\, \frac{\partial I(\lambda)}{\partial \lambda}, \quad (5)$$

where $\phi = f\, B \cos\gamma$ is the longitudinal magnetic flux density, f is the filling factor, B is the field strength, γ is the inclination of the field with respect to the vertical, $C = 4.6686 \times 10^{-13} \lambda_0^2 \bar{g}$ is a proportionality constant that depends on the central wavelength λ_0 and the effective Landé factor $\bar{g}$ of the transition, and I represents the intensity profile. The units of ϕ are Mx cm^{-2} when λ_0 is expressed in Å.

The longitudinal magnetic flux density is obtained from a least-squares minimization of the form

$$\frac{\partial}{\partial \phi}\left[\sum_i \left(V_i + \phi C \frac{\partial I}{\partial \lambda}_i\right)^2\right] = 0, \quad (6)$$

which uses all the wavelength samples across the profile (index i) and is therefore more accurate that determinations based on single magnetogram measurements. This calculation is repeated for each pixel and each spectral line separately. The final result is

$$\phi = -\frac{\sum_i \frac{\partial I}{\partial \lambda}_i V_i}{C \sum_i (\frac{\partial I}{\partial \lambda}_i)^2}. \quad (7)$$

To estimate the uncertainty caused by photon noise we simulated a data set containing only Gaussian noise with a standard deviation of $1.7 \times 10^{-3}\, I_{\rm c}$. The analysis of this data set using Equation (7) leads to a Gaussian-shaped histogram for the magnetic flux density which is centered at 0 and has a standard deviation of $\sigma_\phi = 3.5$ Mx cm^{-2}.

In Figure 3, we check the assumption made on the Zeeman regime. The plot shows an histogram of the ratio between the magnetic flux densities derived from Fe I 630.15 and 630.25 nm. Only the Stokes V spectra at the footpoints of the loops having amplitudes above 5 times the noise level have been considered. As can be seen, the histogram is narrow and peaks at 1. The figure also shows a scatter plot of the magnetic flux densities obtained with the two lines. The fact that most of the points are located near the diagonal implies that in the majority of cases both spectral lines measure the same magnetic flux. This strongly supports the idea that the fields are weak.

4. EMERGENCE OF SMALL-SCALE MAGNETIC LOOPS IN THE QUIET SUN

During 28 hr of observations we have detected the appearance of 69 loop-like structures in the 2.″7 × 40.″6 region scanned with the *Hinode* SP. Table 2 summarizes their properties. The observed loops followed very similar evolution patterns. In this section, we describe specific cases to illustrate the emergence process, distinguishing between loops that rise to the chromosphere and loops that remain low-lying.

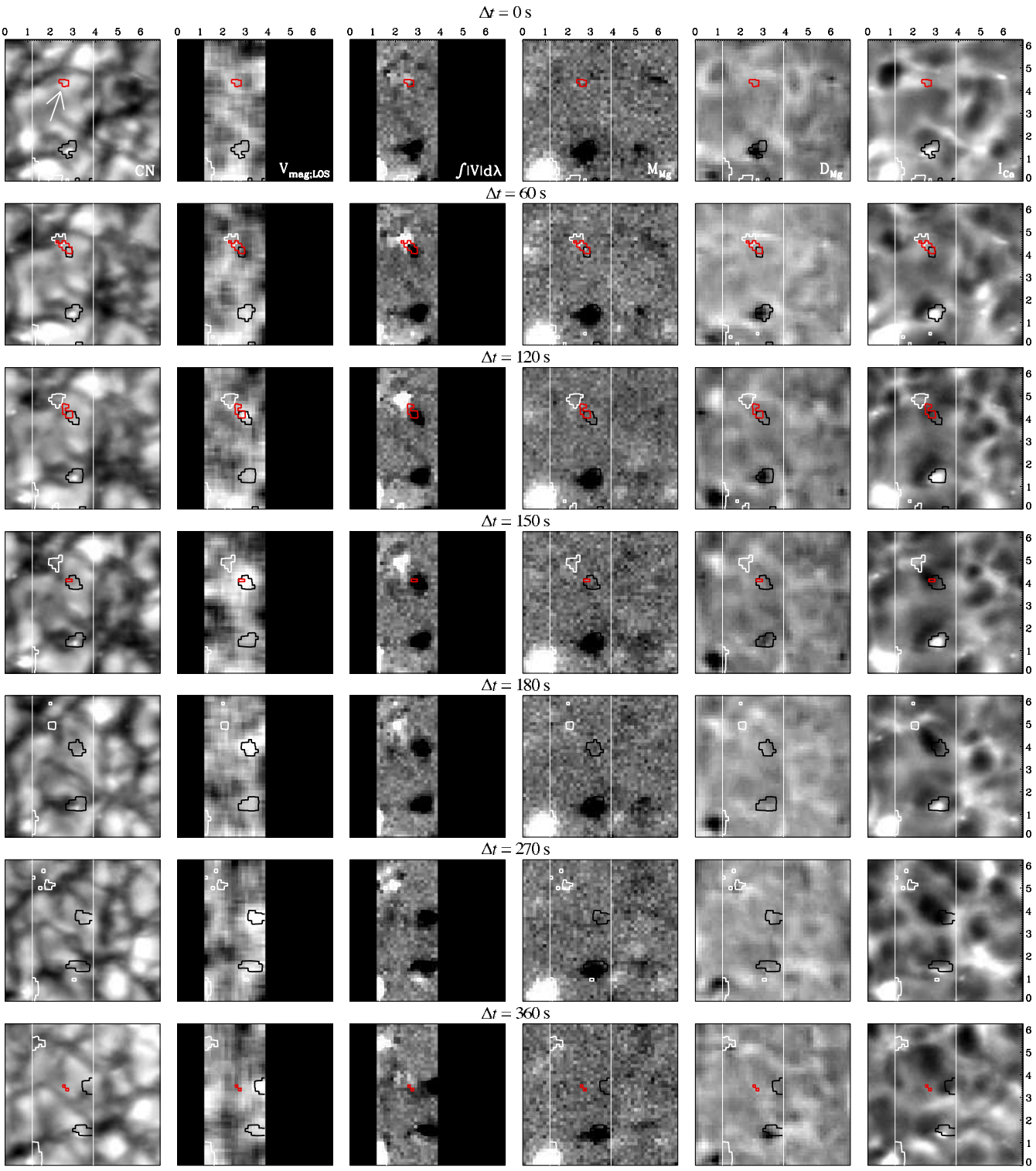

Figure 4. Evolution of the small-scale magnetic loop ml09 that emerges in the photosphere and reaches the chromosphere. The panels show, from left to right, CN intensity, Fe I 630.25 nm Stokes *V* zero-crossing velocity (scaled to ±4 km s^{-1}, with upflows being light), total circular polarization in Fe I 630.25 nm (clipped to ±0.1 pm), magnetic flux density from Mg I b 517.3 nm (scaled to ±22.7 Mx cm^{-2}), LOS velocity from the Mg I b Dopplergram (scaled between −0.5 and 0 km s^{-1}, with stronger downflows appearing darker), and Ca II H line-core intensity. The vertical white lines represent the SP scan. The scales in the horizontal and vertical axes are arcsec. Red contours indicate areas with linear polarization signals in Fe I 630.25 nm larger than 0.22 pm. Black and white contours represent circular polarization signals in the photosphere stronger than ±0.1 pm. Blue and turquoise contours show magnetic flux densities from the Mg I b magnetograms larger than ±13.6 Mx cm^{-2}. The *x*- and *y*-axis are in arcsec.

4.1. Magnetic Loops Emerging up to the Chromosphere

One of the clearest examples of a loop that reached the chromosphere was loop ml09, observed on 2007 September 25 at 14:39 UT. Its evolution is summarized in Figures 4 and 5. Each row represents a time step, for a total of 1020 s. From left to right we show CN filtergrams, photospheric LOS velocities derived from the Stokes *V* zero-crossing shifts of Fe I 630.25 nm, total circular polarization maps in Fe I 632.05 nm, magnetic flux densities computed from Mg I b 517.3 nm, LOS velocities at the

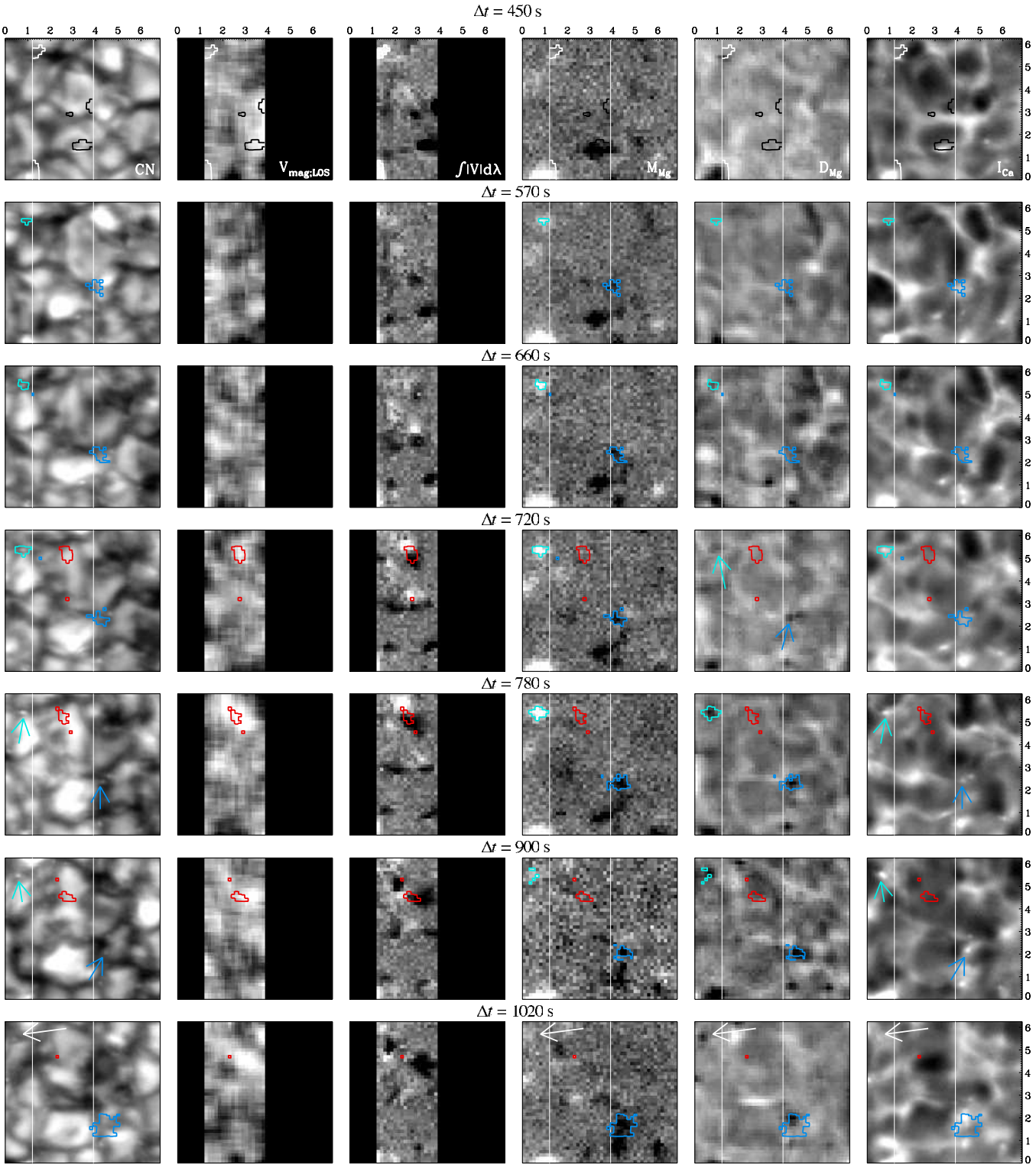

Figure 5. Continuation of Figure 4.

height of formation of the Mg I b line, and Ca II H line-core filtergrams. Positive velocities indicate upflows. Note that the time steps are not evenly spaced; rather, we have adjusted them to better describe the various phases of the process.

The red contours mark regions of large linear polarization signals in Fe I 630.25 nm. When the footpoints of the loop are visible in the photosphere, we plot contours of Fe I 630.25 nm circular polarization in black and white for the negative and positive signals, respectively. When the footpoints are only visible in the Mg I b magnetogram we plot them in blue and turquoise.

The first row of Figure 4 shows the emergence of linear polarization above a granule (see the white arrow in the CN filtergram). It is caused by the horizontal part of the loop reaching the photosphere. The footpoints are not yet visible but will appear 30 s later, very close to the patch of linear

polarization. At $\Delta t = 60$, the loop is completely formed. It emerges in a granular region, perhaps because the upward granular motions help the field lines to rise from below the solar surface (Cheung et al. 2007). The LOS velocity maps show photospheric upflows at the position of the footpoints, confirming that the loop is rising. For the moment, however, the magnetic field remains in the lower photosphere: we do not observe circular polarization signals in the Mg I b magnetograms or brightenings in Ca II H that could be associated with the loop. Interestingly, the strong photospheric network element with negative polarity located toward the bottom of the scan, at a height of about one fourth of the displayed FOV, is well observed both in the Mg I b magnetograms and the Ca filtergrams, and will remain so during most of the time sequence. This nicely illustrates the capabilities of our observations: magnetic structures that are visible in the Fe I polarization maps but not in Mg I b or Ca II H are intrinsically lower in the solar atmosphere.

Between $\Delta t = 150$ s and $\Delta t = 180$ s the linear polarization signals disappear below the noise. The positive footpoint has drifted to an intergranular lane and is concentrated, whereas the negative footpoint continues to be rooted in the granule and is more diffuse. The distance between them increases steadily. We still see upward motions in the photospheric velocity maps. Since the loop moves to higher layers, it is reasonable to conclude that the linear polarization disappears because the apex of the loop leaves the formation region of the 630 nm lines. However, no traces of the loop are detected yet in Mg I b or Ca II H.

At $\Delta t = 270$ s, weak circular polarization signals co-spatial with the photospheric footpoints are observed in the Mg I b magnetograms for the first time. This indicates that the loop has reached the upper photospheric/lower chromospheric layers where the central part of the Mg I b line forms. Interestingly, the Mg I b Dopplergram exhibits downflows of about -0.4 km s^{-1} at the position of the positive footpoint. The downflows could represent plasma moving along the legs of the loop as the whole structure reaches high atmospheric layers. These motions may be essential for the loop to get rid of part of its mass before it can emerge into a less dense medium.

At $\Delta t = 570$ s, the loop is nearly out of the region scanned by the SP. The signals in the Mg I b magnetogram are much more intense and correspond to footpoints rooted in intergranular lanes. From now on the distance between the footpoints will increase, but at a slower rate than when they were crossing granular structures. This inflection point can be seen in Figure 6, where we plot the footpoint separation as a function of time. The distance is computed only when the two footpoints are visible, both in the 630 nm maps (squares) and in the Mg I b magnetograms (triangles). In the first 500 s of the loop evolution, the distance between the footpoints increases linearly at a rate of 5.9 km s^{-1}. Therefore, the mean velocity of the footpoints is 2.95 km s^{-1}, a value compatible with the motion of the granular plasma. The linear increase of the separation with time is a common feature of the loops and indicates that they do not undergo a free random walk (otherwise the distance would increase with the square root of time). Toward the end of the loop evolution the separation rate slows down, coinciding with the arrival of the footpoints to intergranular lanes. Summarizing, the loop emerges in a granule and the horizontal granular motions drive the magnetic field lines to the closest intergranular space, where strong downdrafts capture and stabilize them. When this happens, the separation between the footpoints is about 4000 km.

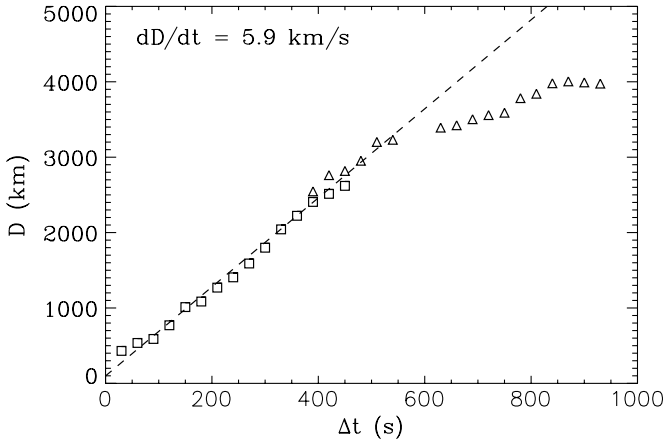

Figure 6. Footpoint separation as a function of time for the loop displayed in Figure 4. The initial time corresponds to the appearance of the linear polarization signal (the top of the loop). The distances between the footpoints in the Fe I 630 nm polarization maps and the Mg I b magnetograms are indicated with squares and triangles, respectively. The linear fit corresponds to the first 500 s of the loop evolution.

At $\Delta t = 660$ s, the footpoints are clearly visible in the Mg I b magnetogram and exhibit downflows in the Mg I b Dopplergram. The whole structure is rising because the footpoints continue to separate. However, no brightenings are detected in the Ca II H filtergrams. We mention in passing that a new loop appears in the FOV at this time, close to the site of emergence of the other loop. They show linear polarization signals in between opposite polarities, which makes it easy to identify.

At $\Delta t = 780$ s, the loop has reached the chromosphere since we observe two Ca II H brightenings associated with the footpoints (in Figure 5, the contours have been substituted by arrows for clarity). The legs of the loop still show downflows in the Mg I b Dopplergrams and, for the first time, bright points are observed in the CN images at the position of the footpoints.

The last panels of Figure 5 display the beginning of the loop decay. The positive footpoint is very weak, although it still shows downflows at the height of formation of the Mg I b measurements. It will disappear below the noise level, together with the downdrafts, at the end of the sequence. The negative footpoint approaches a negative polarity patch with which it will eventually mix. The negative footpoint shows downflows and is associated with a bright point in Ca II H. These features will survive the disappearance of the footpoint thanks to the interaction with the network element.

4.2. Low-Lying Magnetic Loops

In this section we present a typical example of a loop which does not show chromospheric signatures and thus remain low lying. Figure 7 shows all the data available for this loop (ml23), arranged as in Figure 4.

In the first frame, a patch of linear polarization is observed to emerge at the border of a granule (see the white arrow). The footpoints can already be detected in the intergranular lane, but they are very weak. At this time, the photospheric velocity map exhibits a patch of upflows at the position of the loop, confirming its rise through the solar atmosphere.

At $\Delta t = 90$ s the loop reaches its largest extent (520 km) while the upflows start weakening. The linear polarization and the upward plasma motions are almost gone by $\Delta t = 120$ s. In the next frame, at $\Delta t = 150$ s, the loop is no longer seen. The evolution of the loop is so rapid that it appears and disappears

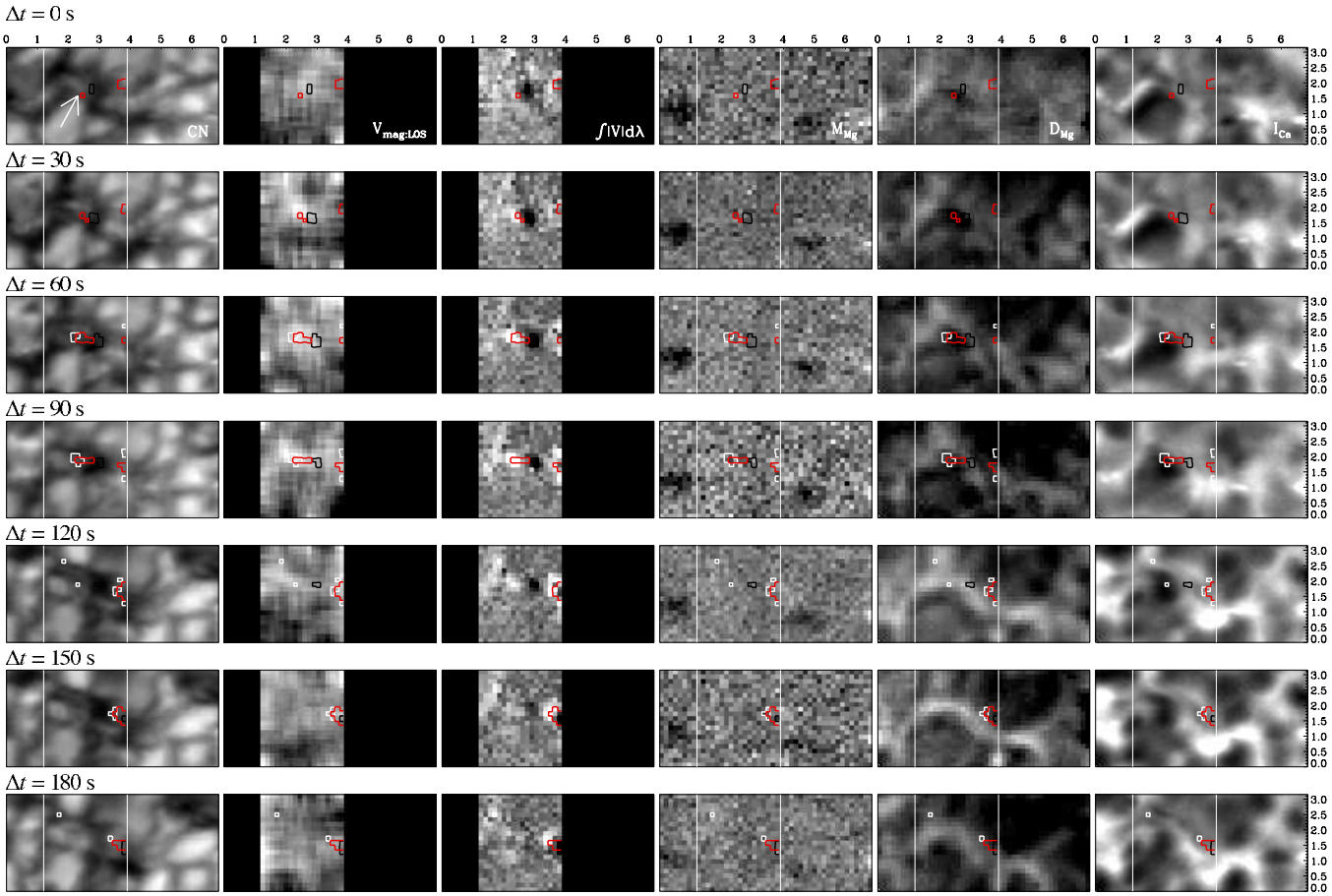

Figure 7. Evolution of the small-scale magnetic loop ml23 that never reached chromospheric heights. The loop appeared on 2007 September 26 at 11:48 UT. The panels are arranged in the same way as in Figure 4.

almost at the same place. Interestingly, the footpoints never approach each other. This rules out submergence below the solar surface as the cause of the loop disappearance.

All the loops that stay in the photosphere show very similar behaviors. In general, they evolve very quickly, disappearing not far from the region where they emerged. None of these loops exhibit downflows in the Mg I b line or brightenings in the CN or Ca filtergrams.

5. EFFECTS IN THE UPPER CHROMOSPHERE

In the previous section, we have seen that small-scale magnetic loops in the quiet Sun may rise through the atmosphere and reach the layers where the central part of the Mg I b 517.3 nm line is formed. Some of them also produce Ca II H brightness enhancements. In this context, the question naturally arises as to the maximum height that these structures can attain. Are they able to reach the upper chromosphere or even the corona?

Here we use the Hα observations of the DOT to provide a partial answer to this question. Unfortunately, there is little overlap between the *Hinode* and DOT measurements because of bad seeing conditions. Nevertheless, for one of the loops detected by *Hinode* there is simultaneous coverage from the DOT. We use these data to attempt to observe the rise of the loop to the upper chromosphere. The analysis is not complete and must be refined with EUV and X-ray observations tailored to the detection of such magnetic structures in the hot corona. It has not been possible to include in this paper the analysis of the *Hinode* X-ray data due to the error expected in the alignment of the X-ray and SP data.

The loop observed simultaneously by *Hinode* and the DOT (ml20) appeared on 2007 September 26, at 09:06 UT. In Figure 8, we show its evolution in the photosphere/temperature minimum region using the Fe I 630.25 nm circular polarization maps and the Mg I b magnetograms (first and second columns, respectively). The figure also displays Hα line-core filtergrams, as well as Hα Dopplergrams at $\pm$0.35 Å and $\pm$0.7 Å from the line center. If the loop reaches the layers where Hα is formed, it should first appear in the fifth column, then in the fourth, and finally in the third.

The loop emerged as a small patch of linear polarization at the border of a granule ($\Delta t = 0$ s, not shown). Its subsequent evolution is similar to that of the loop considered in Figure 4. The footpoints of the loop are detected in the photosphere for the first time at $\Delta t = 180$ s. The whole structure shows upflows in the Stokes V zero-crossing maps, indicating its ascent. Unfortunately, the negative footpoint is close to the border of the FOV scanned by the SP and soon disappears from the photospheric maps. The loop becomes visible in the Mg I b magnetograms at $\Delta t = 390$ s. At this time, there is clear signal in the negative footpoint and weaker polarization in the positive leg. At $\Delta t = 780$ s both footpoints show stronger magnetogram signals but the distance between them has not increased. The ascent of the loop to the chromosphere is associated with downflows in the Mg I b Dopplergram and brightenings in the Ca II H line-core images. The Fe I and Mg I b signals start fading

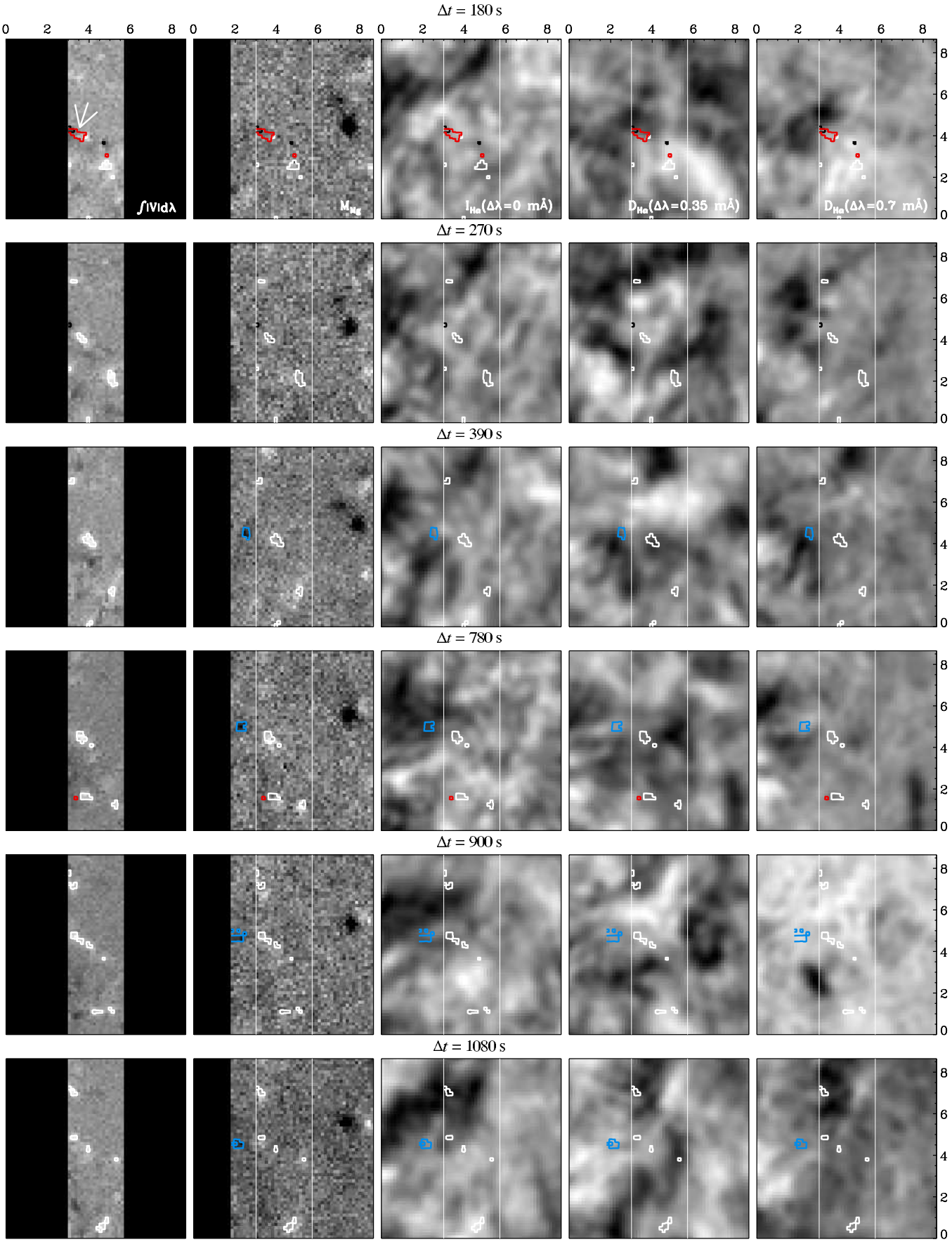

Figure 8. Simultaneous observations of the magnetic loop ml20 emerging in the quiet Sun by *Hinode* and the Dutch Open Telescope. The loop appeared on 2007 September 26 at 09:06 UT. From left to right: circular polarization map in Fe I 630.25 nm, magnetic flux density from the Mg I b magnetograms (scaled to ±22.7 Mx cm^{-2}), Hα line-core image, and Hα Dopplergrams at $\Delta\lambda = \pm 0.35$ and $\Delta\lambda = \pm 0.7$ Å from the line center, respectively.

at $\Delta t = 900$ s until the loop disappears simultaneously from the low and the upper photospheric layers.

The Hα line-core images and the Dopplergrams do not show any particular feature that could be associated with the appearance of an arch filament system in the chromosphere. It is important to remark that the maximum separation between the footpoints of this loop was only 760 km. It may well be that a larger separation is required for the apex of the loop to reach the upper chromosphere. In fact, excessive magnetic tension might prevent the field lines from rising. Keeping in mind these considerations, we do not discard that magnetic loops with larger separations may be seen in future Hα observations.

6. PHYSICAL PROPERTIES OF THE EMERGING LOOPS

In this section, we characterize the physical properties of the small-scale magnetic loops observed with *Hinode*. Weak examples and loops appearing close to strong network elements or in crowded areas are omitted from the analysis to maintain the quality of the results. This leaves us with 33 loops, which represents 48% of the total sample.

Table 2 lists the basic parameters of the loops, including lifetimes (Δt), maximum distances between footpoints ($D_{\rm max}$), speed at which the footpoints separate initially ($V_{\rm D}$), total magnetic fluxes (Φ_{630}), and maximum flux densities (ϕ_{630}) in the photosphere, estimations of maximum magnetic flux densities at the height of formation of the Mg I b measurements ($\phi_{\rm Mg}$), and an estimation of the largest downflows detected in the Mg I b Dopplergrams ($V_{\rm Mg}$). The lifetime is the time elapsed between the appearance and disappearance of the polarization signals. When two numbers are given, the first indicates the time passed until one of the footpoints interacts with a neighboring magnetic element. The second is the time of disappearance proper; if it is accompanied by an asterisk, then the polarization signatures of the loop were still visible at the end of the observations. To compute the total magnetic flux we define the footpoints as those regions where the flux density is larger than $3\,\sigma_\phi$ at the position of the loop. The value of Φ_{630} reported in Table 2 is the maximum flux detected in one of the footpoints during the loop evolution, and the error indicates the uncertainty in Φ_{630} caused by photon noise.

The last four columns of Table 2 give the time intervals between the appearance of the loops in the photosphere and their detection in the Mg I b magnetograms, the Mg I b Dopplergrams, the Ca II H line-core images, and the CN filtergrams. We consider that a loop is present in any of these maps when at least one of the footpoints shows up clearly. The two numbers in each column correspond to the positive footpoint (left) and the negative one (right).

As can be seen in Table 2, there is a wide range of loop parameters. The lifetimes vary from some 2 minutes up to 40 minutes, although most of the loops disappear in less than 10 minutes. The maximum separation between the footpoints is a strong function of the lifetime and ranges from ~500 km to 4000 km. Many loops reach horizontal dimensions comparable to, or larger than, those of granules. The initial velocity of separation between the footpoints does not seem to have any relationship with the other parameters listed in the table. Values of 1–4 km s^{-1} are typical. As already mentioned, the separation speed tends to decrease when the footpoints reach the intergranular space, likely because horizontal motions there are not as vigorous as in the interior of granular cells.

The longitudinal magnetic fluxes measured in the footpoints range from 2×10^{16} to 2×10^{17} Mx at the level of formation of the Fe I 630 nm lines.[4] Therefore, the loops have smaller fluxes than ephemeral regions and should be placed at the lower end of the flux distribution observed in emerging active regions. The magnetic flux density in the footpoints is typically 20–40 Mx cm^{-2}. To infer the magnetic field strength from the magnetic flux density values we need to know the filling factor of the field lines that build the loop structure and their inclination. The footpoints should be relatively vertical because of geometrical reasons. Assuming that the fields occupy most of the resolution element, i.e., that the magnetic filling factor is close to unity the field strength of the loops can be estimated to be of order 10–100 G. Only if the filling factor is much smaller than unity would the field strength increase to kG values.

An important result is that 23% of the loops are detected in the Mg I b magnetograms after their appearance in the photosphere (16 cases out of 69). It takes an average of 5 minutes for the loops to move from the photosphere to the height at which the Mg I b line forms, although faster and slower ascents have been observed too. All the loops detected in the Mg I b magnetograms develop downflows at the same heights. In addition, 15% of the loops are seen as bright points in Ca II H line-core filtergrams. This means that an important fraction of the magnetic flux that emerges into the photosphere reaches the chromosphere. As they travel upward, the loops are observed in the Fe I magnetograms, the Mg I b magnetograms, the Mg I b Dopplergrams, the Ca II H line-core images, and the CN filtergrams (in this order).

By contrast, 77% of the loops never make it to the chromosphere. We have been unable to identify any parameter determining whether a given loop will rise or not. This includes the total magnetic flux and the magnetic flux density. However, low-lying loops tend to have lifetimes shorter than 500 s and separations smaller than 500 km. Thus it may simply be that they do not last long enough to reach high atmospheric layers. Further work is clearly needed to explain why a substantial fraction of the loops remain low-lying. Also, the relation between these structures and the transient horizontal fields described by Ishikawa & Tsuneta (2009) should be investigated, given their similar lifetimes and magnetic topologies.

7. SITES OF EMERGENCE, EVOLUTION, AND TILT ANGLES

The observations described above demonstrate that magnetic fields do emerge into the quiet solar atmosphere in the form of small-scale loops, confirming the results of Martínez González et al. (2007) and Centeno et al. (2007). The loops are detected as a patch of linear polarization flanked by two circular polarization signals of opposite polarity. In nearly all the cases the linear polarization appears before or at the same time as the Stokes V signals, as can be expected from Ω-shaped loops rising through the atmosphere. Only in two cases out of 69 we have detected linear polarization after the loop had already disappeared. In those cases, the footpoints approached each other. This behavior is compatible with a loop that emerges and then submerges in the photosphere, or with a "magnetic bubble," i.e., a circle of magnetic field lines.

The long duration of our time series has permitted us to discover the existence of emergence centers in which several loops appear one after the other. For example, there is a $8'' \times 3''$ region of the solar surface where we have detected

[4] Note that the magnetic flux of ml24 is 1.9×10^{18} Mx, considerably larger than the rest of values. This might be an artifact caused by the difficult separation of ml24 and the strong network element with which it interacts.

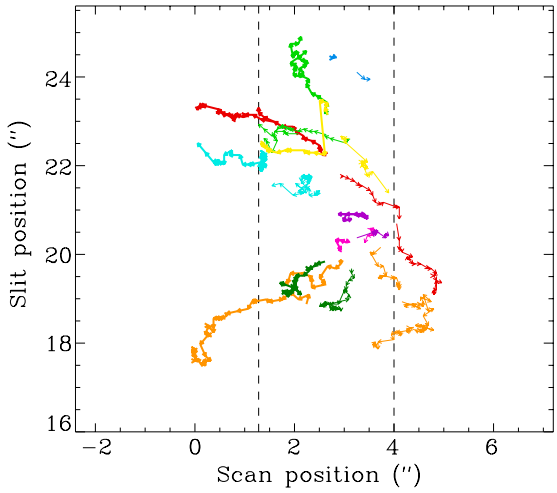

Figure 9. Trajectories of nine loops that appeared on 2007 September 25. Thick and thin lines indicating the positive and negative footpoints of each loop. The paths in red, blue, light green, yellow, turquoise, pink, orange, dark green, and violet correspond to loops ml09__ml17 in Table 2, respectively. The vertical dashed lines mark the FOV of the SP observations at 630 nm.

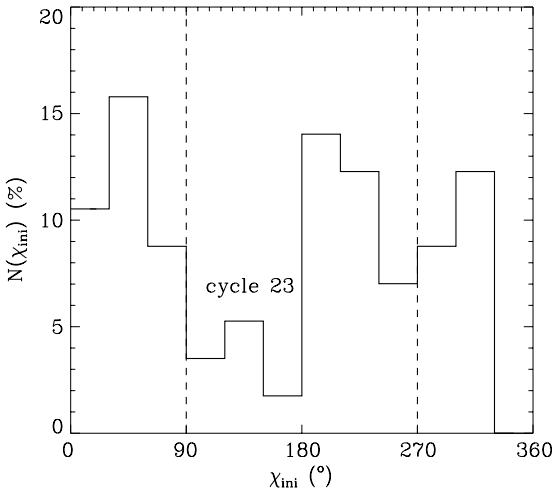

Figure 10. Distribution of initial tilt angles for 66 emerging loops. Angles between 90° and 270° imply that the positive polarity patch is the leading one (in the sense of rotation), consistent with Hale's rules in the northern hemisphere during solar cycle 23.

nine events in a time interval of 1 hr. The complete set of observations covering this period is provided in the online journal as an mpeg animation. Some of the loops even appear at the very same position. The example shown in Figure 4 belongs to this area. The existence of emergence centers may have important consequences for the origin of the loops. These regions act as subsurface reservoirs of magnetic flux that is transferred intermittently to the photosphere by an as-yet-unkwnown mechanism.

The loops generally emerge in granules or at their edges, although there are exceptions of loops appearing in dark areas. As the loops emerge, the footpoints separate and the linear polarization fades away. In most cases, the footpoints do not describe rectilinear trajectories. Figure 9 shows the paths followed by the two polarities of the loops observed on 2007 September 25 (loops ml09 to ml17 in the Table 2). The red curves correspond to the example discussed in Figures 4 and 5. In this case, the footpoints described quite a rectilinear path, similarly to emerging active regions and ephemeral regions. However, the majority of loops show more complicated trajectories. The reason is that, in general, they emerge in granules and drift toward the closest intergranular lane. When the footpoints reach the intergranular space they stay there and are passively advected by the flow. This creates complicated trajectories. The important point, however, is that the magnetic field is sufficiently weak as to be pushed and moved around by the granular flow, but *without being destroyed in the process*.

During their evolution, the loops interact with other magnetic flux concentrations that cross their paths. If the loops stay long in the photosphere, the footpoints cancel with elements of opposite polarity or are absorbed by patches of the same polarity. Loops that experience a fast evolution have more probabilities of avoiding other magnetic elements and often disappear without undergoing any interaction.

In seeking the origin of the loops it is of interest to determine the magnetic orientation of their footpoints. If the loops are caused by the global solar dynamo, one may expect a regular ordering of the footpoints at the moment of emergence. This is what happens in active regions, where the signs of the leader and follower polarities are governed by Hale's rules (see, e.g., Stix 2002). All the loops considered here appeared in the northern hemisphere during solar cycle 23. In that cycle, leader polarities were positive in the northern hemisphere and negative in the southern hemisphere. Figure 10 shows an histogram of the orientation of our small-scale emerging loops. The tilt angle is defined to be the angle between the solar equator and the line joining the positive footpoint with the negative one, measured from the west. The angles compatible with the orientation of sunspot polarities during solar cycle 23 in the northern hemisphere are those between 90° and 270°. Even if the statistical sample is not very large, the loops seem to have nearly random orientations. Thus, we conclude that they do not obey Hale's polarity rules, much in the same way as the shortest-lived ephemeral regions (Martin & Harvey 1979; Hagenaar et al. 2003).

8. DISCUSSION AND CONCLUSIONS

Recent observations of Hanle-sensitive lines (Trujillo Bueno et al. 2004) and Zeeman-sensitive lines (Martínez González et al. 2008b; Orozco Suárez et al. 2007; Lites et al. 2008; Ishikawa & Tsuneta 2009) suggest that a significant fraction of the quiet Sun is occupied by magnetic fields. Apparently, these fields are weak and isotropically distributed in inclination (Martínez González et al. 2008a). One way to shed light on their nature is to study how they emerge in the surface and what their contribution is to the energy budget of the solar atmosphere.

On granular scales, magnetic flux appears in the solar photosphere as transient horizontal fields (Ishikawa & Tsuneta 2009) and small-scale magnetic loops (Martínez González et al. 2007; Centeno et al. 2007). We have studied the latter in detail using seeing-free observations made by *Hinode*. In 28 hr of *Hinode* data we have detected 69 small-scale loops emerging in a quiet Sun region of size $2\farcs7 \times 40\farcs6$ at the disk center. The occurrence rate is thus 0.02 events hr^{-1} arcsec^{-2}. The loops show clear spectropolarimetric signatures with a central region of linear polarization and two patches of circular polarization of opposite polarity.

The longitudinal flux observed in each footpoint ranges from 2×10^{16} to 2×10^{17} Mx, with an average of $\sim 9.1 \times 10^{16}$ Mx. This means that the loops represent the smallest emerging flux regions detected to date (ephemeral regions have fluxes above 10^{18} Mx; Zwaan 1987). The rate at which magnetic flux is

Table 2
Physical Properties of the Small-Scale Emerging Magnetic Loops

Name	Date (09/07)	t_{ini} (UT)	Δt (s)	D_{max} (km)	V_D (km s^{-1})	Φ_{630} (Mx)	ϕ_{630} (Mx cm^{-2})	ϕ_{Mg} (Mx cm^{-2})	V_{Mg} (km s^{-1})	Δt_{SP-Mg} (s)	$\Delta t_{SP-down}$ (s)	Δt_{SP-Ca} (s)	Δt_{SP-CN} (s)
ml01	25	13:36:15	240	800	3.9	$4.6\times10^{16}\pm1\times10^{15}$	23.2 ± 0.6						
ml02	25	13:35:45	150/1020	1220	4.0	$1.5\times10^{17}\pm2\times10^{15}$	24.8 ± 0.6						
ml03	25	13:37:45	330	560	0.9	$7.6\times10^{16}\pm1\times10^{15}$	29.7 ± 0.4						
ml04	25	13:46:15	60/480	690	1.7	$8.2\times10^{16}\pm1\times10^{15}$	23.1 ± 0.9						
ml05	25	13:45:15	240	790	1.1	$1.1\times10^{17}\pm1\times10^{15}$	23.0 ± 1.1						
ml06	25	13:36:15	180	910	6.0	$3.6\times10^{16}\pm9\times10^{14}$	16.6 ± 0.6						
ml07	25	13:54:15	90	490	1.4	$3.5\times10^{16}\pm8\times10^{14}$	8.1 ± 0.3						
ml08	25	13:41:45	630	800	6.2	$3.9\times10^{16}\pm1\times10^{15}$	25.3 ± 0.6						
ml09	25	14:39:30	960/1200	4000	3.9	$1.3\times10^{17}\pm1\times10^{15}$	32.8 ± 0.4	15.0±1.1	−1.1	270/540	270/750	780/780	780/1230
ml10	25	14:42:00	120	560	1.7	$1.5\times10^{16}\pm6\times10^{14}$	18.6 ± 1.1						
ml11	25	14:51:00	300/2550*	1670	2.5	$1.2\times10^{17}\pm1\times10^{15}$	32.3 ± 0.6	10.4±1.0	−0.58	180/450	180/450	420/660	/660
ml12	25	14:51:00	300/2550*	2040	0.7	$1.3\times10^{17}\pm1\times10^{15}$	24.3 ± 0.4	8.3 ± 0.8		690/750			
ml13	25	15:04:00	660/1230	1440	2.1	$7.8\times10^{16}\pm1\times10^{15}$	28.9 ± 0.5	28.6 ± 0.9	−0.70	390/390	690/	750/	690/
ml14	25	15:06:00	180	480	3.7	$6.1\times10^{16}\pm1\times10^{15}$	23.4 ± 0.4						
ml15	25	15:14:00	360/1590*	3170	0.5	$2.0\times10^{17}\pm2\times10^{15}$	29.8 ± 0.4	5.4 ± 0.5	−0.91	330/330	570/420	750/420	690/570
ml16	25	15:24:30	510	790	0.9	$1.3\times10^{17}\pm2\times10^{15}$	34.2 ± 0.4	7.3 ± 0.5	−0.59	240/240	270/270		
ml17	25	14:50:30	90	620	1.0	$5.5\times10^{16}\pm1\times10^{15}$	22.6 ± 0.5						
ml18	26	08:32:00	510/1110*	990	1.1	$1.1\times10^{17}\pm1\times10^{15}$	33.5 ± 0.4						
ml19	26	08:23:30	660	1670	3.1	$6.2\times10^{16}\pm1\times10^{15}$	18.1 ± 0.4	10.0 ± 0.9	−0.33	/180	/180	/210	/180
ml20	26	09:06:00	1050	1450	2.2	$1.5\times10^{16}\pm6\times10^{14}$	15.7 ± 0.9	5.0 ± 0.4	−0.38	390/360	510/390	570/420	600/390
ml21	26	09:47:30	240	700	2.8	$3.8\times10^{16}\pm9\times10^{14}$	23.7 ± 0.6						
ml22	26	11:24:00	1380*	1570	0.9	$2.4\times10^{17}\pm2\times10^{15}$	42.2 ± 0.3	11.8 ± 1.1	−0.48	360/450	600/750	630/750	
ml23	26	11:48:00	150	520	3.6	$3.3\times10^{16}\pm9\times10^{14}$	23.1 ± 0.6						
ml24	26	12:16:00	120/390	830	3.4	$1.9\times10^{18}\pm2\times10^{15}$	75.8 ± 1.1						
ml25	26	12:28:00	1230	2840	0.1	$2.0\times10^{16}\pm7\times10^{14}$	21.4 ± 0.8	7.50 ± 0.8	−0.56	210/420	540/630	690/690	
ml26	27	09:25:00	1110	760	0.9	$7.0\times10^{16}\pm1\times10^{15}$	32.7 ± 0.6	26.7 ± 0.8	−0.42	270/270	540/		
ml27	27	11:08:00	420	960	4.5	$8.6\times10^{16}\pm1\times10^{15}$	30.6 ± 0.6						
ml28	27	12:20:30	90	670	0.9	$3.0\times10^{16}\pm9\times10^{14}$	15.2 ± 0.5						
ml29	27	12:26:30	1110	2290	4.0	$1.7\times10^{17}\pm2\times10^{15}$	27.2 ± 0.4	14.5 ± 0.8	−0.49	150/150	450/390	/450	
ml30	28	11:28:30	300/750	1300	0.9	$7.8\times10^{16}\pm1\times10^{15}$	24.4 ± 0.5						
ml31	28	11:38:00	180	1560	1.5	$7.8\times10^{16}\pm1\times10^{15}$	19.0 ± 0.3						
ml32	28	12:32:30	720/720	710	1.5	$1.9\times10^{17}\pm1\times10^{15}$	44.6 ± 0.4	19.0 ± 0.5		240/240		360/	330/
ml33	29	08:39:00	240/630	860	2.4	$2.1\times10^{17}\pm1\times10^{15}$	42.2 ± 0.3						
Mean			**741**	**1234**	**2.2**	$\mathbf{9.13\times10^{16}}$	**26.1**	**13.0**	**−0.60**	**295**	**406**	**513**	**514**

carried to the quiet photosphere by the loops can be estimated to be 1.1×10^{12} Mx s^{-1} arcsec^{-2}, or 1.1×10^{24} Mx over the solar surface per day. This is about half the value derived by Lites et al. (1996) for horizontal internetwork fields, but still enormous (see van Driel-Gesztelyi 2002 for a comparison with the flux emergence rates in active and ephemeral regions).

In the photosphere, the linear polarization associated with the top of the loop disappears soon, while the circular signals tracing the loop legs are observed to separate with time. This behavior is consistent with field lines moving upward through the solar atmosphere. Also the upflows observed in the Stokes V zero-crossing velocities at the position of the footpoints confirm the ascent of the loops. 23% of the loops are detected in Mg I b magnetograms that sample the upper photosphere or the temperature minimum region (say, 400 km above the continuum forming layer). There is a time delay of about 5 minutes between the first detection in the photosphere and the appearance in the Mg I b magnetograms, implying an ascent speed of the order of 1 km $^{-1}$. Some of the loops continue to travel upward and become visible in Ca II H line-core filtergrams as small brightness enhancements. Thus, a fraction of the loops are able to reach the low chromosphere, carrying magnetic flux with them.

The rise of small-scale magnetic loops may provide an efficient mechanism to transfer substantial amounts of energy from the photosphere to the chromosphere. This would support claims by Trujillo Bueno et al. (2004) and Ishikawa & Tsuneta (2009) that the tangled fields of the quiet Sun store sufficient energy to heat the chromosphere. A related question is whether the small-scale loops rise up to the transition region or even the corona. The observations required to answer this question are quite challenging due to the different spatial resolutions attainable with present-day optical, EUV, and X-ray instruments, but should be pursued.

About 77% of the loops that appear in the solar surface never rise to the chromosphere. These loops have the shortest lifetimes and show the smallest footpoint separations; other than that, they do not differ from those reaching higher layers. Usually, they disappear close to their emergence sites. The fields associated with these loops might represent the tangled quiet Sun fields deduced from Hanle measurements (Stenflo 1987; Manso Sainz et al. 2004), but a definite conclusion cannot be made without studying the compatibility of Hanle and Zeeman measurements.

What is the origin of the small-scale magnetic loops? One possibility is that they are created by the solar dynamo at the bottom of the convection zone, as part of a larger toroidal flux tube. Cheung et al. (2007) presented three-dimensional MHD simulations of the last stages of the emergence of one such tube. They placed a horizontal tube at the top of the convection zone,

just beneath the photosphere. When the initial magnetic flux is smaller than $\sim 10^{18}$ Mx, the tube is not sufficiently buoyant to rise coherently against the convective flows and fragments. At the surface, the process of flux emergence occurs on very small spatial scales (typically 1000–2000 km) and short time scales (5 minute). These properties are compatible with our observations. Thus, the small-scale loops we have detected may simply be the result of weak flux tubes distorted by the granulation as they emerge from the convection zone into the photosphere. The fragmentation of the tubes might explain why there are emergence centers where loops appear recurrently one after the other. A preliminary analysis of the footpoint orientations suggests that the loops do not show a tendency to be aligned according to Hale's rules. This can be regarded as a considerable difficulty against the idea that the origin of the loops is the solar dynamo. However, it may also be a natural consequence of the interaction of the tube's fragments with the near-surface granular convection if it removes all the information carried originally by the tube.

Another possibility is that the magnetic loops represent flux recycled from decaying active regions. In a sense, the MHD simulations of Abbett (2007), Isobe et al. (2008), and Steiner et al. (2008) model such a process, because all of them assume an initial magnetic field in the computational box which could be provided by decaying active regions. In the simulations, the field evolve and interact with the granular flows. This interaction creates a significant amount of horizontal fields, even if the initial field is purely vertical. Moreover, the simulations show the emergence of magnetic loops on granular scales. The loops are less coherent than classical flux tubes and do not connect to deeply rooted field lines. In this scenario, the magnetic fields of the quiet Sun, and thus the emergence events we have described, would be the consequence of local processes acting on the remnants of decaying active regions.

Yet another possibility is that the loops represent submerged horizontal magnetic fields carried to the surface by the upward motions of granules or by magnetic buoyancy, as modeled by Steiner et al. (2008). Even in that case, the origin of such submerged fields would be unknown.

Nowadays, we do not have enough observational constraints to distinguish between a surface dynamo or an "exploding" magnetic flux tube emerging from the solar interior. Determining the nature of the magnetic loops observed in internetwork regions is important for a better understanding of the magnetism of the quiet Sun and its role in the heating of the solar atmosphere. Future efforts should concentrate on the solution of these problems. In addition to high-resolution photospheric observations, polarization measurements in the chromosphere are required to track the evolution of the loops with height. These data can now be provided by two-dimensional spectrometers such as IBIS, CRISP, or IMaX.

We thank Andrés Asensio Ramos, Pascal Démoulin, and Rafael Manso Sainz for very helpful discussions, and Véronique Bommier for carefully reading the manuscript. We are grateful to all the observers who participated in the *Hinode* Operation Plan 14, both at ISAS/JAXA and at the ground-based telescopes. Special thanks are due to Suguru Kamio (NAOJ) for coordinating the campaign and to Peter Sütterlin (Utrecht University) for making the observations at the Dutch Open Telescope and reducing them. *Hinode* is a Japanese mission developed and launched by ISAS/JAXA, with NAOJ as a domestic partner, and NASA and STFC (UK) as international partners. It is operated by these agencies in cooperation with ESA and NSC (Norway). Part of this work was carried out while one of us (M.J.M.G.) was a Visiting Scientist at the Instituto de Astrofísica de Andalucía. We acknowledge financial support from the Spanish MICINN through projects ESP2006-13030-C06-02, PCI2006-A7-0624, and AYA2007-63881, and from Junta de Andalucía through project P07-TEP-2687.

REFERENCES

Abbett, W. P. 2007, ApJ, 665, 1469
Brault, J., & Neckel, H. 1987, Spectral Atlas of Solar Absolute Disk-averaged and Disk-center Intensity from 3290 to 12510 Å, ftp.hs.unihamburg.de/pub/outgoing/FTS-atlas
Carlsson, M., et al. 2007, PASJ, 59, 663
Centeno, R., et al. 2007, ApJ, 666, 137L
Cheung, M. C. M., Schüssler, M., & Moreno Insertis, F. 2007, A&A, 467, 703
Domínguez Cerdeña, I., Sánchez Almeida, J., & Kneer, F. 2006, ApJ, 646, 1421
Hagenaar, H. J., Schrijver, C. J., & Title, A. M. 2003, ApJ, 584, 1107
Ishikawa, R., & Tsuneta, S. 2009, A&A, 495, 607
Ishikawa, R., et al. 2007, A&A, 481, L25
Isobe, H., Proctor, M. R. E., & Weiss, N. O. 2008, ApJ, 679, L57
Khomenko, E. V., Collados, M., Solanki, S. K., Lagg, A., & Trujillo Bueno, J. 2003, A&A, 408, 1115
Kosugi, T., et al. 2007, Sol. Phys., 243, 3
Landi degl'Innocenti, E. 1992, in Solar Observations: Techniques and Interpretation, ed. F. Sánchez, M. Collados, & M. Vázquez (Cambridge: Cambridge Univ. Press), 73
Lites, B. W. 2002, ApJ, 573, 431
Lites, B. W., Elmore, D. F., & Streander, K. V. 2001, in ASP Conf. Ser. 236, Advanced Solar Polarimetry—Theory, Observation, and Instrumentation, ed. M. Sigwarth (San Francisco, CA: ASP), 33
Lites, B. W., Leka, K. D., Skumanich, A. P., Martínez Pillet, V., & Shimizu, T. 1996, ApJ, 460, 1019
Lites, B. W., Skumanich, A. P., Rees, D. E., & Murphy, G. A. 1988, ApJ, 330, 493
Lites, B. W., et al. 2008, ApJ, 672, 1237
Manso Sainz, R., Landi Degl' Innocenti, E., & Trujillo Bueno, J. 2004, ApJ, 614, 89
Martin, S. F. 1988, Sol. Phys., 117, 243
Martin, S. F., & Harvey, K. L. 1979, Sol. Phys., 64, 93
Martínez González, M. J., Asensio Ramos, A., López Ariste, A., & Manso Sainz, R. 2008a, A&A, 479, 229
Martínez González, M. J., Collados, M., Ruiz Cobo, B., & Beck, C. 2008b, A&A, 477, 953
Martínez González, M. J., Collados, M., Ruiz Cobo, B., & Solanki, S. K. 2007, A&A, 469, 39
Orozco Suárez, D., Bellot Rubio, L. R., del Toro Iniesta, J. C., & Tsuneta, S. 2008, A&A, 481, 330
Orozco Suárez, D., et al. 2007, ApJ, 670, 61
Rutten, R. J., Hammerschlag, R. H., Bettonvil, F. C. M., Sütterlin, P., & de Wijn, A. G. 2004, A&A, 413, 1183
Stein, R. F., & Nordlund, Å. 2006, ApJ, 642, 1246
Steiner, O., Rezaei, R., Schaffenberger, W., & Wedemeyer-Böhm, S. 2008, ApJ, 680, 85
Stenflo, J. O. 1987, Sol. Phys., 114, 1
Stix, M. 2002, The Sun: An Introduction (Berlin: Springer)
Trujillo Bueno, J., Shchukina, N., & Asensio Ramos, A. 2004, Nature, 430, 326
Tsuneta, S., et al. 2008, Sol. Phys., 249, 167
van Driel-Gesztelyi, L. 2002, ESASP, 505, 113
Zwaan, C. 1987, ARA&A, 25, 83
Zwaan, C. 1985, Sol. Phys., 100, 397